International Journal of Fracture (2006) 140:213–233
DOI 10.1007/s10704-005-6103-0

Sliding along frictionally held incoherent interfaces in homogeneous systems subjected to dynamic shear loading: a photoelastic study*

G. LYKOTRAFITIS and A. J. ROSAKIS**
Graduate Aeronautical Laboratories, California Institute of Technology, Mail Stop 105-50, 1200 E. California Blvd, Pasadena, CA 91125, USA
***Author for correspondence (E-mail: rosakis@aero.caltech.edu)*

Received 1 July 2005; accepted in revised form 20 December 2005

Abstract. An experimental investigation was conducted to study dynamic sliding at high strain rates along incoherent (frictional) interfaces between two identical plates. The plates were held together by a uniform compressive stress, while dynamic sliding was initiated by an impact-induced shear loading. The case of freely-standing plates with no external pressure was also investigated. The dynamic stress fields that developed during the events were recorded in a microsecond time scale by high-speed photography in conjunction with classical dynamic photoelasticity. Depending on the choice of experimental parameters (impact speed and superimposed static pressure), pulse-like and crack-like sliding modes were observed. Visual evidence of sub-Rayleigh, intersonic and even supersonically propagating pulses were discovered and recorded. Unlike classical shear cracks in coherent interfaces of finite strength, sliding areas in frictional interfaces seem to grow at various discrete speeds without noticeable acceleration phases. A relatively broad loading wave caused by the interference between the impact wave and the preexisting static stress field was observed emanating from the interface. There was a cusp in the stress contours at the interface, indicating that the propagation speed was slightly faster along the interface than in the bulk. The observed propagation speeds of the sliding tips were dependent on the projectile speed. They spanned almost the whole interval from sub-Rayleigh speeds to nearly the sonic speed of the material, with the exception of a forbidden gap between the Rayleigh wave speed and the shear wave speed. Supersonic trailing pulses generating Mach lines of different inclination angles, emanating from the sliding zone tips, were discovered. In addition, behind the sliding tip, wrinkle-like opening pulses were observed for a wide range of impact speeds and confining stresses. They always traveled at speeds between the Rayleigh wave speed and the shear wave speed of the material.

Key words: Crack-like sliding, dynamic frictional sliding, homogeneous system, incoherent interface, pulse-like sliding, wrinkle-like pulse

1. Introduction

Many engineering procedures involve frictional sliding along incoherent interfaces between two deformable solids. Examples include moving machinery surface interaction (both macro and micromachinery), material processing (e.g. cutting), the failure of fiber reinforced composites (e.g. fiber pullout) as well as earthquake dynamics (fault rupture). However, a unified framework for quantifying the wide range of

* Symposium on Physics and Scaling in Fracture held during the ICF11 (2005) in Turin.

observed dynamic frictional phenomena is only beginning to emerge. The classical Amontons–Coulomb description of friction states that shear stress at an interface is proportional to the normal stress, with the coefficient of proportionality being the coefficient of friction. In this classic description of friction, two coefficients of friction are identified: a static coefficient of friction that governs the onset of sliding and a dynamic coefficient of friction that characterizes the behavior during sliding.

From the microscale point of view an evolving population of contacts and their local deformation, phase transition and fracture and the presence of various lubricants, appear to play an important role in setting the static and dynamic coefficient of frictions as well as in governing the transition between them. From the phenomenological point of view, rate and state models of friction have been introduced, e.g. Dieterich (1979), Ruina (1983), Rice and Ruina (1983), Linker and Dieterich (1992), Prakash and Clifton (1993), and Prakash (1998). Such models, based on experimental observations, attempt to describe the local microprocesses of surface interaction through appropriately chosen state variables.

Rate and state models of friction have come to the fore because they substantially influence the nature (mode) and stability of sliding. There are two widely accepted approaches to the description of dynamic sliding (Rice, 2001). The most classic approach uses elastodynamic shear crack models (behind the leading edge of sliding, the surfaces continuously slide and interact through contact and friction). More recently, models that describe sliding as 'self-healing' slip pulse have been introduced (behind the leading edge of the sliding, there is sliding for a finite length followed by surface locking).

Classic dynamic fracture theories (Freund, 1990; Broberg, 1999) of growing shear cracks have many similarities to the frictional sliding process. These theories treat the rupture front as a distinct point (sharp tip crack). The crack-like rupture of coherent interfaces, separated by similar and dissimilar solids subjected to dynamic shear loading, has been the subject of extensive experimental, numerical, and analytical investigations in the past years and has been summarized by Rosakis (2002) in a recent review. Of relevance to the present study is the persistent occurrence of intersonic shear rupture in coherent interfaces separating identical monolithic solids. Such a phenomenon was first observed experimentally by Rosakis et al. (1999) and by Coker and Rosakis (2001) and has been numerically modeled by Needleman (1999) using the cohesive element methodology and by Hao et al. (2004) using a mesh-free finite element methodology. A special rupture speed of $\sqrt{2}\,c_S$ as the speed separating regions of unstable and stable intersonic shear crack growth has also been identified (Burridge et al., 1979; Freund, 1979; Samudrala et al., 2002a). Atomistic models of intersonic shear rupture (Abraham and Gao, 2000; Abraham, 2001; Gao et al., 2001) as well as field observations of intersonic rupture events during recent large crustal earthquakes (Archuleta, 1984; Olsen et al., 1997; Hernandez et al., 1999; Bouchon et al., 2001; Lin et al., 2002; Bouchon and Valle, 2003; Ellsworth et al., 2004; Xia et al., 2004, 2005) have demonstrated the remarkable length scale persistence (over 11 orders of magnitude) of the intersonic rupture phenomenon and of the main features observed by laboratory experiments and by continuum theory.

The traditional view of seismology has also been based on crack-like models of rupture (Das, 1985). Inversions of seismic data for slip histories indicate, however, that earthquake slip often occurs as narrow propagating pulses with rise time one

order of magnitude smaller than the event duration. Heaton (1990) suggested that the inferred results can be generated by self-healing sliding pulses associated with strongly velocity-weakening friction and consequent low-frictional heat. Theoretical and numerical investigations have shown that propagation of self-sustained slip pulse along an interface of deformable bodies is possible under some conditions (Zheng and Rice, 1998; Cochard and Rice, 2000; Ranjith and Rice, 2001; Ben-Zion and Huang, 2002). In general, narrow slip pulses can be generated during dynamic sliding along interfaces by strongly velocity-weakening friction on a homogeneous system (same material across the interface), by strong fault zone heterogeneities (Rice, 2001) or by variations in normal stress along the rupture interface. All of the above conditions (velocity weakening, heterogeneities and bimaterial contrast) can produce slip pulses with low dynamic stress at the active part of the slip and provide satisfactory solution to the heat flow paradox. An extensive discussion of the subject is presented by Nielsen and Madariaga (2003). We finally note that finite element calculations have been carried out by Coker et al. (2005) for a configuration similar to our experimental setup. These simulations show that generation of slip pulses along an interface characterized by a rate and state dependent frictional law is feasible.

The possibility of generating interface waves in incoherent frictionless contact between two dissimilar solids, when separation does not occur, was first investigated by Achenbach and Epstein (1967). These 'smooth contact Stonely waves' (also known as slip waves or generalized Rayleigh waves) are qualitatively similar to those of bonded contact and occur for a wider range of material combinations. Comninou and Dundurs (1977) found that self-sustained slip waves with interface separation (detachment waves or wrinkle-like slip pulses) can propagate along the interface of two similar or different solids, which are pressed together. The constant propagation speed of these waves was found to be between the Rayleigh wave speed and the shear wave speed of the slowest material. Weertman (1980) obtained a 2-D self-sustained wrinkle-like slip pulse propagating at the generalized Rayleigh wave speed along a bimaterial interface governed by Coulomb friction when the remote shear stress was less than the frictional strength of the interface. Finite-difference calculations of Andrews and Ben-Zion (1997) show the propagation of wrinkle-like pulses along a bimaterial interface governed by Coulomb friction. Particle displacement in a direction perpendicular to the fault is much larger in the slower material than in the faster material, resulting in a separation of the interface during the passage of the slip pulse. Anooshehpoor and Brune (1999) discovered such waves in rubber sliding experiments (bimaterial system consisted of two rubber blocks with different wave speeds). The above mentioned detachment waves are radically different from the Schallamach waves (Schallamach, 1971) which propagate very slowly compared to the material wave speeds. Slow detachment front waves have also been recently detected by Rubinstein et al. (2004).

As we see, there is a debate about the different high-rate phenomena that occur at the interface of two incoherent half-planes during frictional sliding and there is not enough experimental evidence so far which would help to analyze the problem. The majority of the existing experimental studies use a large time scale and they are concerned with developing qualitative and/or quantitative relationships between time averaged friction data and various governing parameters. Unfortunately, most dynamic friction laws obtained using various experimental configurations and appa-

ratus lack the reproducibility of friction data (survey by Ibrahim, 1994). The results of these experiments are multi-branched friction versus slip velocity curves, which even for the same material and the same experimental apparatus depend not only on the properties of the frictional interface but also on the dynamic properties of the apparatus, such as mass, stiffness and damping. This suggests that the friction data obtained in the course of stick-slip motions are not an intrinsic property of the surfaces in contact but they are greatly affected by several of the dynamic variables involved in each particular experimental setup. Prakash (1998) employs a plate-impact pressure-shear friction experiment to investigate dynamic frictional response of a sliding interface on a microsecond time-scale. The experimental results, deduced from the response to step changes imposed on the normal pressure at the frictional interface, reinforce the importance of including frictional memory in the development of the rate-dependent state variable friction models. However, this setup is not able to provide information about the stress field developed in the specimen or to shed light on the interfacial process during dynamic sliding.

The purpose of the present work is to study experimentally the high-rate events which occur at the interface of two identical elastic plates during sliding caused by an asymmetric impact shear loading. Using photoelasticity in conjunction with high-speed photography, the nature of dynamic rupture was investigated in a microsecond time-scale. We were able to capture in real time significant effects like loading waves, sliding initiation and propagation, Mach lines indicating supershear sliding tip speed, slip pulses, and transition from pulse-like to crack-like sliding. Also, behind the sliding tip, a very robust fringe structure which is related to a wrinkle-like pulse was identified. In addition, the speeds of the sliding tips and the interface waves were obtained. The variation of these speeds with the impact speed and the confining stress was also investigated.

2. Material and specimen configuration

Experiments were performed to investigate the nature of dynamic frictional sliding along the incoherent interface of two plates made of identical material. The experimental results were recorded in a microsecond time scale and the initiation and evolution of sliding were explored. The material used was Homalite-100, a mildly rate sensitive brittle polyester resin that exhibits stress induced birefringence with an optical coefficient $F_\sigma = 22.6\,\mathrm{KN/m}$. The isochromatic fringe patterns formed in the Homalite plates were clearly visible at impact speeds higher than 9 m/s. Homalite-100 is a very well characterized material, which at strain rate of $10^3\,\mathrm{s}^{-1}$ exhibits almost purely elastic properties. The longitudinal, shear and Rayleigh wave speeds in Homalite are $C_\mathrm{P} = 2583\,\mathrm{m/s}$, $C_\mathrm{S} = 1249\,\mathrm{m/s}$ and $C_\mathrm{R} = 1155\,\mathrm{m/s}$, respectively. The above values were obtained by ultrasonic measurement, using pressure and shear transducers operating at 5 MHz, which give the wave speeds in the 3-D bulk material. In the performed experiments, however, the configuration was plane stress, since plate specimens 76.2 mm high, 139.7 mm long, and 9.525 mm thick were employed. The plane stress shear wave speeds are identical to the values obtained in the 3-D configuration. The same is true for the Rayleigh wave speed since the contribution in the Rayleigh wave formation comes primarily from the shear wave. However, the plane stress lon-

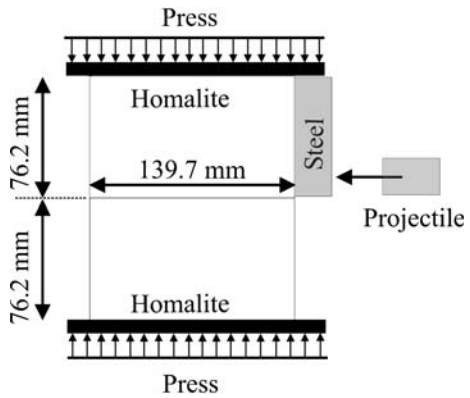

Figure 1. Geometry and loading configuration for a specimen constituted by two identical incoherent plates.

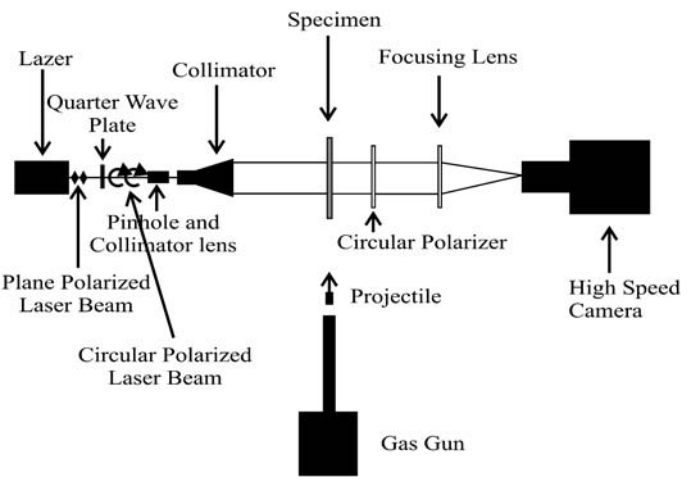

Figure 2. Experimental setup. A circular polarized laser beam passes through the specimen which is subjected to impact shear loading via a projectile fired by a gas gun. The resulting isochromatic fringe patterns are recorded by a high-speed digital camera.

gitudinal wave speed of Homalite-100 is $C_{\mathrm{P}}^{\sigma} = 2187\,\mathrm{m/s}$ and it is different from the corresponding 3-D value.

3. Experimental procedure

The experimental procedure was similar to that used by Rosakis et al. (1999) and by Samudrala and Rosakis (2003) in the investigation of shear crack propagation. The plate specimens were held together by a uniform compressive stress applied by a calibrated hydraulic press (see Figure 1). The asymmetric impact loading was imposed via a cylindrical steel projectile of diameter 25 mm and length 51 mm fired using a gas gun with impact velocities ranging from 9 to 72 m/s. A steel buffer 73 mm high and 25.4 mm long was attached to the specimen at the impact site to prevent shattering and to induce a more or less planar loading wave.

Dynamic photoelasticity was used to extract stress field information. Figure 2 shows a typical experimental setup for dynamic photoelasticity experiments. The photoelastic optical setup was arranged for light field. The isochromatic fringes are contours of maximum in-plane shear stress $\tau_{\max}$ governed by the stress optical law

$$2\,\tau_{\max} = \sigma_1 - \sigma_2 = N\ F_\sigma / h,$$

where F_σ is the stress optical coefficient, h the specimen thickness, σ_1, σ_2 are the principal stresses, and $N = n + 1/2$ (with $n = 0, 1, 2, \ldots,$) is the isochromatic fringe order. A continuous, circular polarized laser beam of 130 mm diameter was transmitted through the specimen and an analyzer. The resulting isochromatic fringe pattern was recorded by a high speed digital camera (Cordin model 220), which is able to record 16 distinct frames at framing rates up to 100 million frames per second. In this experimental work most of the high-speed photography was performed at 250,000 to 1000,000 frames per second. The field of view was wide enough to cover most of the specimen.

The Homalite plate surfaces were used as they came from the cutting machine without undergoing any specific treatment. The average interface roughness was approximately $R_a = 400$ nm. The average roughness R_a is simply the average of the absolute values of the surface height variations z_i measured from the mean surface level. Expressed in equation form, this is $R_a = 1/N \sum_{i=1}^{N} |z_i|$, where N is the number of measurement points. The measurements were performed by a mechanical stylus surface profiler Tencor Alphastep 200.

4. Photoelastic stress field during dynamic sliding of a homalite plate subjected to a constant external compressive stress and different impact speeds

In this section, the influence of the impact speed on the sliding process along incoherent interfaces is investigated. Results are described from a number of experiments, performed at the same external confining stress of 10 MPa and at different impact speeds. The images in Figure 3a shows the isochromatic fringe patterns at selected times for an impact speed of 32.7 m/s. The images at different times are similar indicating that the sliding propagation had reached a more or less steady state. In Figure 3b, our attention is focused on the image (iii) of Figure 3a. The loading wave front arrives from the right. The arrow A shows the position of the longitudinal wave front. A relatively broad fringe pattern (shown just behind point A) having a rib-eye structure emanates from the interface. Since this structure was missing in similar experiments without external pressure (see Section 5), we can safely conjecture that it was caused by the interference of the loading wave with the preexisting confining static pressure. In addition, it is noted that the eye-like fringe structure was not related to the sliding process, since it developed also in simple impact experiments where the specimens did not have any interface and consequently no sliding was allowed.

The impact loading created a horizontal compressive stress σ_{11} in the upper plate, close to the interface. This was the driving stress for the sliding. Because of the Poisson effect, the compressive stress induced a dynamic (inertial) vertical compressive stress, which depended on the impact speed. A very simple calculation, based on the theory

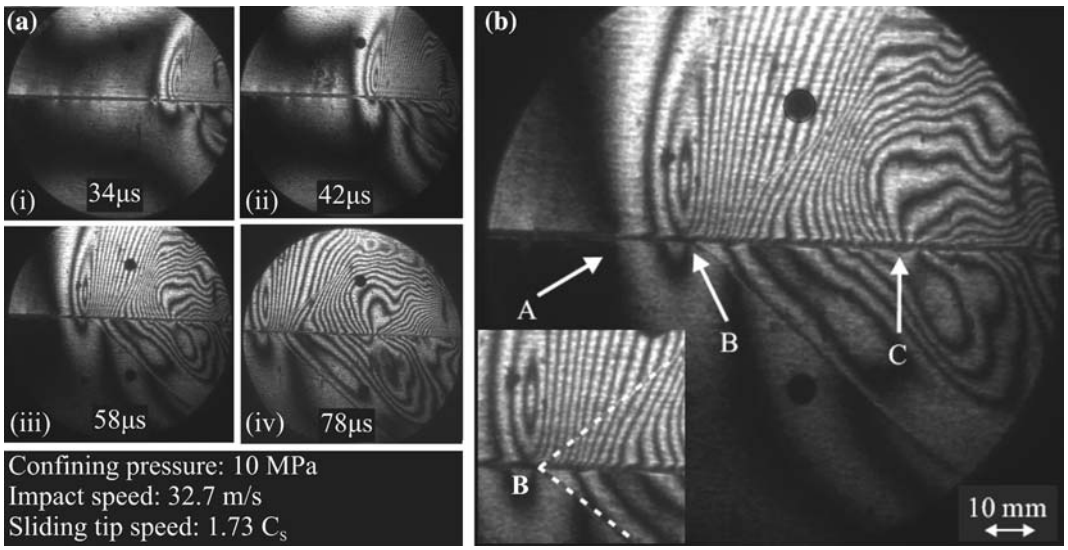

Figure 3. (a) Isochromatic fringes of intersonic sliding propagation at different time instances. (b) The *p*-wave front (A), the sliding tip (B), and the detachment interface wave (C) are shown clearly in the magnification of the fringe pattern (iii).

of 1-D wave propagation in solids, gives that for impact speeds on the order of 40 m/s, the maximum dynamic compressive stress is expected to be on the order of 10 MPa, which is comparable to the confining static stress we used. The dynamic compressive stress was added to the confining stress and the frictional sliding resistance $\tau = f\,\sigma_{22}$ (where f is the dynamic friction coefficient) increased. Consequently, there was a coupling between σ_{11} and the static friction. The compressive stress σ_{11} generated the shear stress, which produced sliding when it overcame the static friction, and at the same time it increased the static friction via the Poisson effect.

The sliding started at point B, where the driving shear stress attained its maximum and became equal to the resisting friction. The sliding propagated intersonically behind the loading wave and a shear Mach cone emanating from the rupture point was formed by a sharp change in the fringe density. The insert of Figure 3b focuses on the region near the propagating tip and a dashed line is drawn along the Mach discontinuity. The position of the longitudinal wave front was measured in each one of the 16 available frames. As it is shown in Figure 4a, the positions followed an almost linear pattern, which means that the *p*-wave speed was constant and the longitudinal wave did not exhibit measurable amount of dispersion within the window of observation of our experiments. A linear interpolation gave a plane stress longitudinal wave speed of 2161 m/s, which is very close to the value 2187 m/s obtained by an ultrasonic measurement as mentioned in Section 3. Using the ultrasonic measurement technique the glassy properties of Homalite-100 are obtained. The fact that both methods give essentially the same value for the longitudinal wave speed means that the strain rate during the impact experiment was high and the specimen did not exhibit any viscoelastic behavior. Independent measurements show that the strain rate was on the order of $1000\,s^{-1}$.

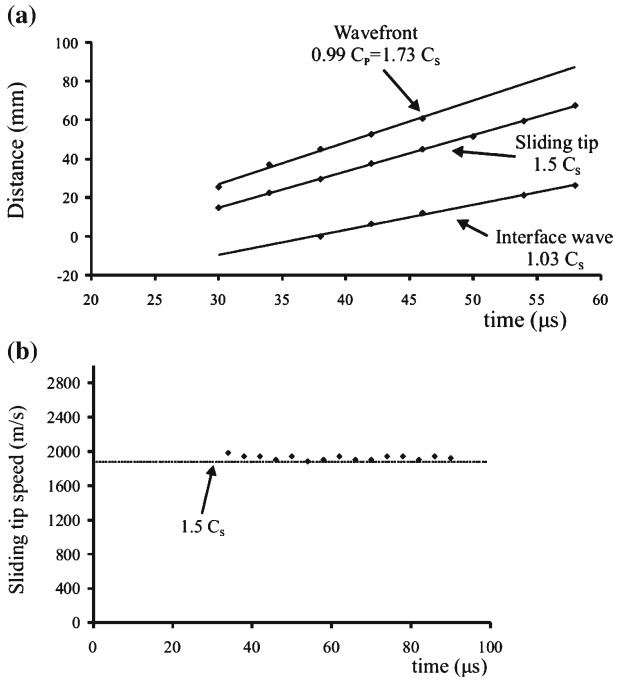

Figure 4. (a) Positions of the longitudinal wave front, the sliding tip and the detachment interface wave as a function of time. (b) Sliding tip speeds at different frames measured using the Mach angle.

The propagation speed of sliding was obtained in two different ways and found to be constant. First we followed the positions of the sliding tip B (see Figure 4a) in different frames. The variation is very well approximated as linear and thus we can conclude that the sliding propagation speed was constant. A linear interpolation gave a sliding tip speed of 1868 m/s $\cong 1.5\,C_S$. Then by using the relation $v = c_s/\sin\theta$, where v is the speed of the sliding tip and θ is the Mach angle, the sliding tip speed at different frames was obtained (see Figure 4b). Again, a constant sliding tip speed within an experimental error is observed. The average value of the sliding tip speed is 1927 m/s $\cong 1.54\,C_S$. Both methods are found to be in agreement to within 3.1 %. The above result was obtained by using the shear wave speed of Homalite measured ultrasonically. Again, the fact that both methods give essentially the same result strengthens the conclusion, drawn from the p-wave propagation speed measurement, that during impact experiments the Homalite specimens do not exhibit viscoelastic behavior.

Some distance behind the sliding tip a fringe structure was formed (point C in Figure 3b). This structure was very robust and it was propagated with a speed of 1288 m/s $\cong 1.03\,C_S$, which is close to the Rayleigh and shear wave speeds of Homalite-100. We also note that in all the experiments performed at different impact speeds and different confining pressures these singularities were traveling at constant speeds between c_R and c_S within an experimental error. Self-sustained interface waves called separation or detachment waves or wrinkle-like pulses have been predicted theoretically by Comninou and Dundurs (1977) in the case of a homogeneous system of two identical plates under compression and by Weertman (1980) in the case of a bimaterial system. Andrews and Ben-Zion (1997) were also able to generate numer-

ically wrinkle-like pulses in a bimaterial fault. Anooshehpoor and Brune (1999) discovered such waves in rubber sliding experiments (bimaterial system consisted of two rubber blocks with different wave speeds). According to the theoretical predictions, the propagation speed of a wrinkle-like pulse is expected to be between the shear wave speed and the Rayleigh wave speed of the plates. The fringe structure, we have identified, is a strong candidate for a wrinkle-like pulse since its propagation speed was within the theoretically obtained speed interval for this pulse. Our conjecture is strengthened furthermore by experimental results obtained on bimaterial interfaces (Lykotrafitis and Rosakis, 2005, submitted). In these experiments photoelasticity was combined with local velocity measurements and it was proved categorically that similar fringe structures were related to detachment interface waves. The above mentioned detachment waves are radically different than the Schallamach waves (Schallamach, 1971), which propagate very slowly compared to the material wave speeds. Other characteristic features in Figure 3b are: (i) a cusp in the stress contours at the interfaces, indicating that the propagation speed is slightly faster along the interface than in the bulk; (ii) the fringe density is higher in the plate where the impact loading was applied, showing that energy is not transferred easily across the interface, and (iii) the fringe discontinuity at the interface shows that there is a relative sliding between the two faces behind the rupture point reflecting the fact that rupture happened in a crack-like mode.

Finally, an important comment on the above-mentioned frictional sliding experiment is that the sliding tip speed and the interface wave speed were constant during the entire observation time. This is a general result and it holds true not only for the previously cited experiment but also for all the experiments performed. The sliding tip speed, the interface wave speed, and the speeds of all the other disturbances or singularities, which are identified in the rest of the paper propagating along the interface, were always constant. This is a strong characteristic of frictional sliding and it agrees with theoretical results (Adams, 1998; Ranjith and Rice, 2001; Rice et al., 2001), which predict constant discrete propagation speeds for all the different disturbances and singularities along the interface.

In Figure 5, isochromatic fringe patterns are shown at three different time instances for the same compressive load of 10 MPa as in the previous experiment and at higher impact speed of 42.2 m/s. The sliding propagated intersonically at approximately $1948\,\text{m/s} = 1.56\,C_S$. Although the general characteristics we encountered at the slower impact speed were still preserved, new features enriched the picture. Behind the loading wave a shear Mach cone was formed. In addition, a second Mach line which was non-parallel to the first one was observed behind the rupture point (Figure 5a). The Mach line was at a shallower slope corresponding to a supershear propagation speed of $2514\,\text{m/s} = 2.01\,C_S$. Non-parallel shock lines imply a highly transient and unstable contact process. Indeed, in Figure 5b the tip of the second Mach line approached the end of the first Mach line. Finally these two points merged as the second point caught up with the first point (see Figure 5c). The sliding continued at the lower speed and thus only one Mach line is observed in the next recorded frames. More detailed views of the rupture process are shown in the inserts of Figure 5a–c. The dual and single shock waves structures are marked with dashed lines. The existence of two Mach lines means that there was onset of sliding at two different points and thus we can conjecture

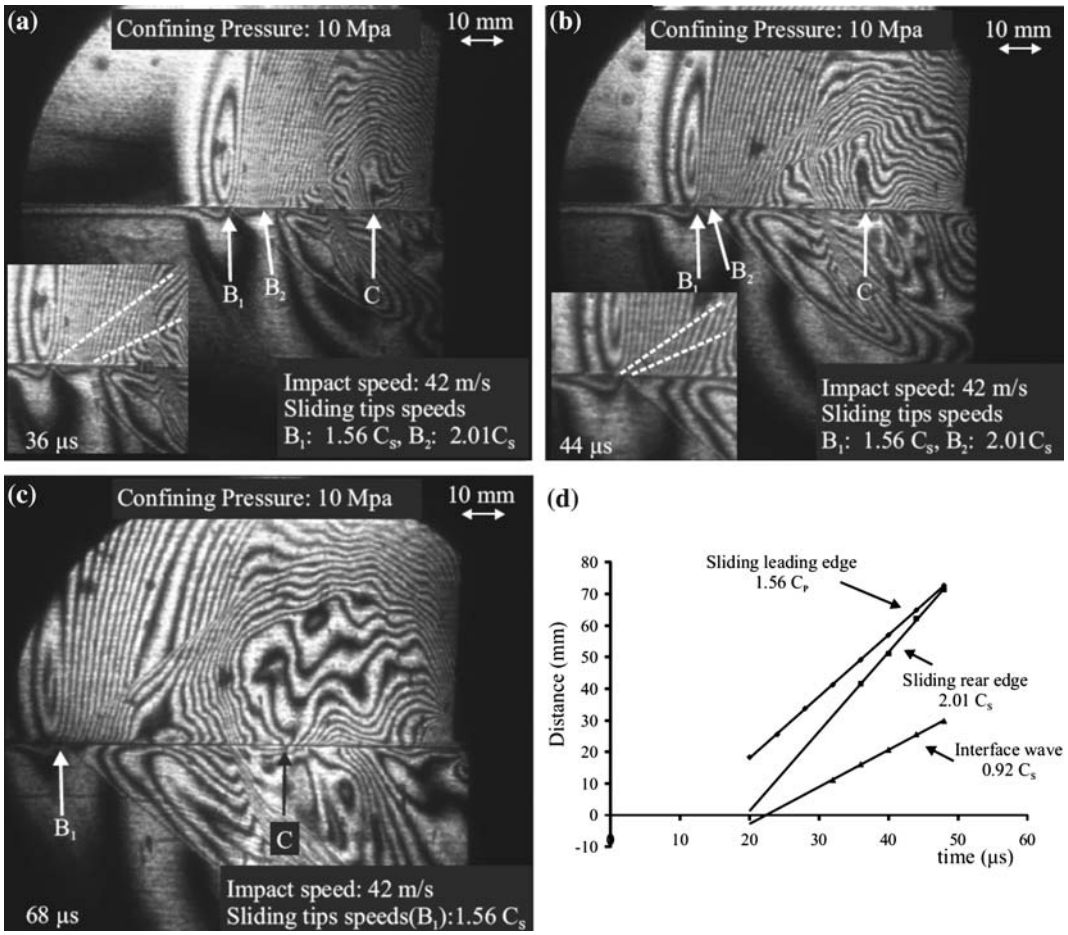

Figure 5. (a–c) Isochromatic fringes of sliding propagation at different time instances. Two sliding tips (B_1 and B_2) were propagating at different intersonic speeds. In the inserts the dual and single Mach lines are marked. (d) Positions of the sliding leading edge, the second sliding tip and the detachment interface wave as a function of time.

that the initial sliding, which started at point B_1 stopped sliding after a while and new sliding started at point B_2. In this way, an unstable sliding pulse was formed between the points B_1 and B_2 followed by a crack-like sliding, which started at point B_2. Behind the second Mach line, the wrinkle-like pulse appeared at point C. It propagated with a speed of $0.92\,C_S$ close to the Rayleigh wave speed of Homalite. Figure 5c shows the position histories of the first and second sliding tips and the detachment interface wave for the case above. It is evident that the second sliding tip moved faster than the first sliding tip and at approximately 50 μs the two points coalesced.

Experiments at higher impact speeds than 42 m/s and at 10 MPa external pressure produce an essentially similar stress distribution as the previous experiment. Significant differences, however, are expected to emerge at lower impact speeds because of the following reason. Rate and state friction laws with strong velocity weakening are employed for describing sliding along uniform interface (Ben-Zion, 2001; Rice, 2001).

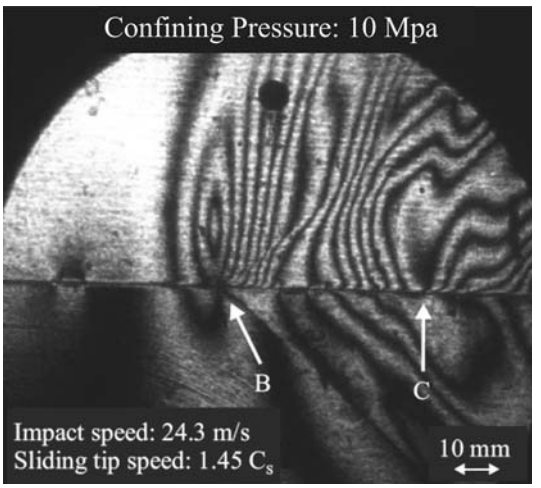

Figure 6. Isochromatic fringes of sliding propagation.

These laws are able to generate self-healing sliding pulses when the overall driving stress is lower than a certain value. In the performed experiments, the driving stress is created by the impact loading. Thus, as we reduce the projectile speed, the driving stress decreases and under a certain value of impact speed the transition from crack-like to pulse-like sliding is anticipated. Pulse-like sliding will definitely create a different stress distribution than crack-like sliding. Another expected change in the fringe pattern is related to the interface wave. Low-impact speeds are not able to create enough horizontal compression stress to overcome the confining stress and to generate wrinkles at the interface. Thus, we do not expect the creation of detachment interface waves at impact speeds lower than a certain value.

Following the above line of thought, we decreased the impact speed to 24.3 m/s while the confining pressure was kept constant at 10 MPa. Figure 6 depicts the photoelastic field at 40 μs after impact. The sliding tip traveled at a supershear speed of $1813\,\text{m/s} = 1.45\,C_S$ and a Mach cone emerged from it. The wrinkle-like pulse formed and propagated at $1228\,\text{m/s} \cong 0.98\,C_S$. Lower impact speeds result in lower dynamic stresses and therefore a lower fringe pattern density is developed than arises at higher impact speeds. Figure 7 shows the fringe pattern at specific times in the cases of four different projectile speeds 19, 13, 11.2 and 9 m/s, where the external pressure was 10 MPa. The density of fringe pattern decreased further. The eye-like structure was traveling at slower speed than the plane stress *p*-wave speed. Thus, the *p*-wave front was well ahead of the eye-like structure and we could not capture it, since we had adjusted the camera timing to record the sliding tip propagation.

In Figure 7a, where the impact speed was 19 m/s, the sliding tip traveled at a supershear speed of $1705\,\text{m/s} \cong 1.36\,C_S$. The wrinkle-like pulse again appeared and it propagated at $1257\,\text{m/s} \cong 1.0\,C_S$, very close to the shear wave speed of Homalite. We observed, however, that as the impact speed decreases the characteristic shape of the wrinkle-like pulse is less prominent and we deduce that the wave was not well formed. As we mentioned before, this is due to the fact that low-impact speeds do not create enough horizontal compression stress to overcome the vertical confining stress and create wrinkles at the interface. At even lower impact speeds, as in the case

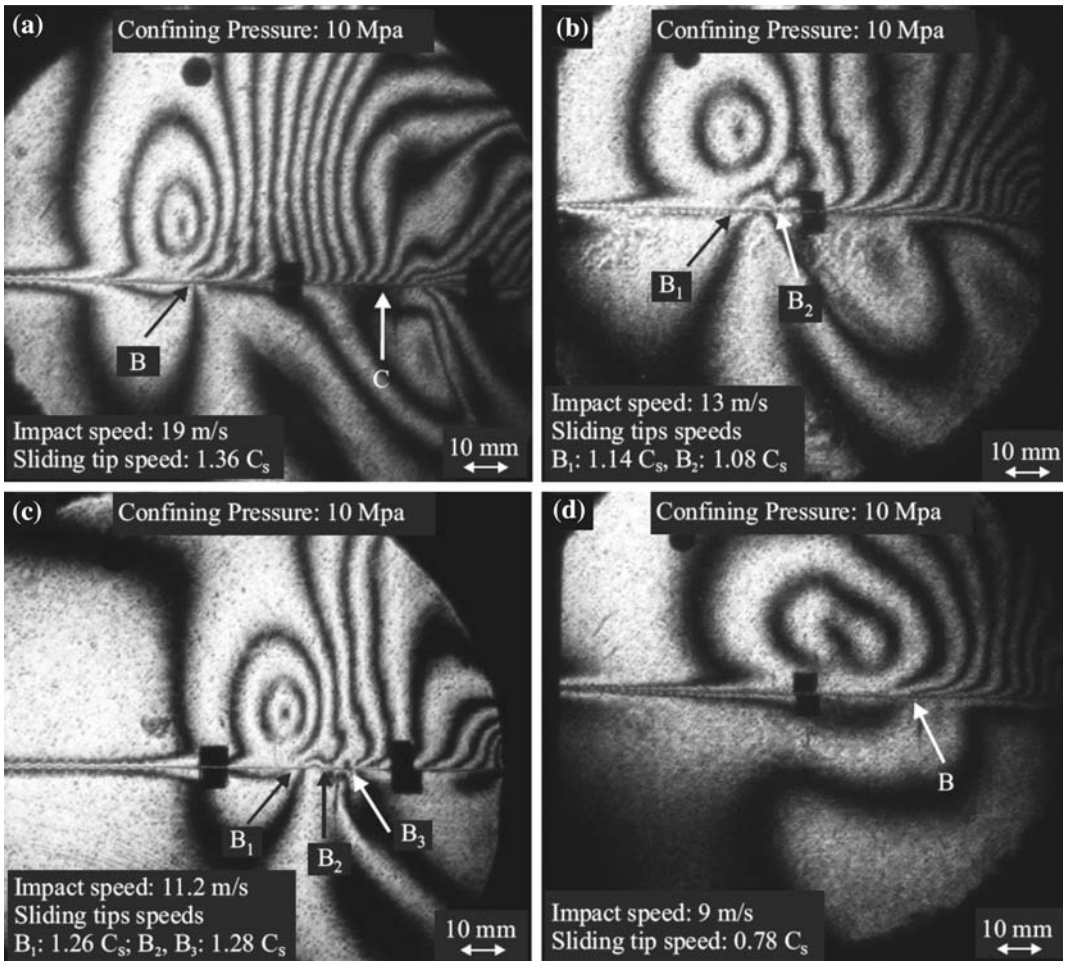

Figure 7. Representative isochromatic fringe patterns from four different experiments of sliding propagation initiated by different impact speeds. The specimens were subjected to the same confining stress.

in Figure 7b–d, the wrinkle-like pulse was not generated. We note at this point that wrinkle-like pulses ware never observed for impact speeds less than 17 m/s and confining stress of 10 MPa.

The photoelastic stress field developed in the case of 13 m/s impact speed is shown in Figure 7b. Two fringe concentration points B_1 and B_2 are observed. The sliding started at point B_1, the end of the eye-like fringe pattern. However at B_2, there was another fringe concentration point which was a second sliding tip. Following B_1 and B_2 at different frames we found that they traveled at constant speeds of $1427\,\text{m/s} \cong 1.14\,C_S$ and $1347\,\text{m/s} = 1.08\,C_S$, respectively. We conjecture that the section B_1B_2 was a self-sustained pulse, which propagated at a supershear speed. The Mach cones are not so prominent because the fringe density is low, and the fringe discontinuity along the Mach lines was not well-formed. However, the two Mach lines can definitely be traced if the kinks of the fringes in the upper plate were to be connected. Sliding speed at point B_1 started to increase from zero value until a maximum

value and then it decreased to a minimum value at point B_2, which is the second sliding tip. At point B_2 a crack-like sliding started, since an almost uniform fringe discontinuity along the interface was formed.

Figure 7c shows the fringe pattern at 70 μs after impact with a projectile of 11.2 m/s speed. Three singular points B_1, B_2, and B_3, appear in the picture. Their sliding speeds were 1573 m/s $\cong 1.26\,C_S$, 1594 m/s $\cong 1.28\,C_S$, and 1586 m/s $\cong 1.28\,C_S$, respectively. Thus, the three points traveled at the same supershear speed within an experimental error. The Mach lines are not so prominent because the fringe density was low. The first tip corresponds to the sliding initiation. Two pulses, B_1B_2 and B_2B_3, were formed and a crack-like sliding initiated at the point B_3.

In all the previous experiments, sliding tip speeds were greater than the shear wave speed. However, lower impact speeds resulted in lower sliding propagation speeds and we expected that as we decreased the projectile speed the sliding tip speed would eventually be subshear. This is the case in Figure 7d. There, a photoelastic stress field generated from an impact with a projectile of 9 m/s speed at 90 μs after impact is shown. A Mach cone was not generated since the sliding tip traveled at a subshear speed of 980 m/s $\cong 0.78\,C_S$.

The variation of the sliding propagation speed with the impact speed at constant uniform confining stress of 10 MPa is shown in Figure 8a. The slowest impact speed we were able to achieve using the gas gun was 9 m/s. At this case and in other cases with impact speeds close to 10 m/s the sliding tip speed was sub-Rayleigh. At impact speeds higher than 11 m/s the sliding edge speed became supershear. We observed that for impact speeds in the range of 20 to 40 m/s, the sliding speed was close to $\sqrt{2}\,c_S$. This is a special rupture speed and it has been shown that it separates regions of unstable and stable intersonic shear crack growth (Samudrala et al., 2002b). When the impact speed increased, the sliding tip speed increased toward the plane stress p-wave speed. It is worth mentioning that no sliding speed was observed in the interval between the Rayleigh wave speed and the shear wave speed of Homalite-100. This experimental observation agrees with theoretical works on steady-state shear crack propagation, which exclude this speed interval based on energetic arguments (Freund, 1990; Broberg, 1999). We also note that the performed experimental sliding tip speed measurements feature high-enough resolution to obtain propagation speeds in the interval between C_R and C_S, if such speeds existed. This is proved by the fact that almost all the recorded speeds of the interface wave were in this speed interval.

The speeds of interface wave at different impact speeds and same confining stress of 10 MPa are shown in Figure 8b. The sliding speed was, within an experimental error, always between the Rayleigh wave and the shear wave speed of Homalite-100. This result favors our conjecture that the interface wave was actually a wrinkle-like pulse, since, as we have already mentioned, the theoretical and numerical analysis on the subject predict the same wave speed limits.

5. Frictional sliding without confining pressure

Experiments at different impact speeds and without external stress applied are presented in this section. Using the above configuration, we were able to observe only the effect of impact loading on the sliding process. Figure 9a shows an instantaneous photoelastic fringe pattern at 92 μs after impact. The projectile speed was 13 m/s.

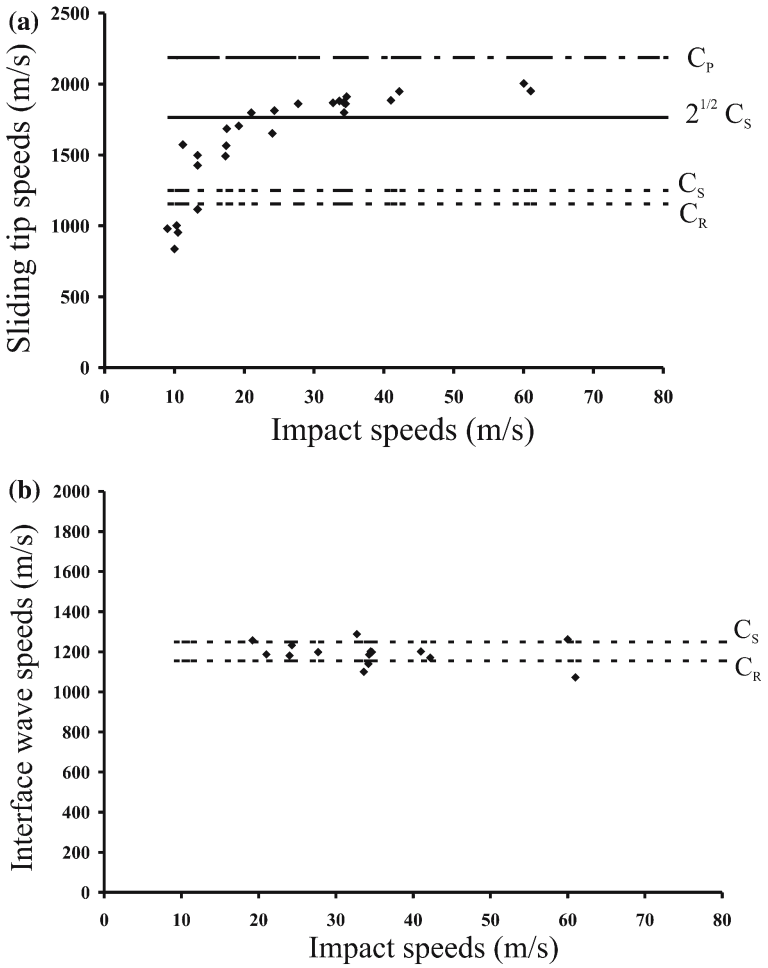

Figure 8. (a) Variation of the sliding tip speed with the impact speed. The confining stress was 10 MPa. (b) The wrinkle-like pulse speed remained between the Rayleigh wave speed and the shear wave speed of Homalite-100, independent of the impact speed.

The fringes at the wave front are almost vertical to the interface, showing that a shear loading was almost obtained. At point C, a fringe structure characteristic of a wrinkle-like pulse is present. We also note that the eye-like fringe pattern was not formed. This proves that the eye-like fringe structure is indeed generated by the interaction between the loading wave and the static confining stress. Regarding sliding, we conjecture that it started almost immediately after the *p*-wave front. However, we cannot identify any sliding tip, since the fringe density is very small.

Another characteristic of the fringe pattern is that the fringes on the left of the wrinkle-like pulse were slightly bent toward the interface. This is more pronounced in Figure 9b, where the impact speed was 24 m/s. The fringes bent toward point B and a fringe concentration point was about to be formed. The wrinkle-like fringe structure was at C and traveled at 1126 m/s $\cong 0.9\,C_S$. We also note that the first three fringes on the left of point B are slightly inclined but they do not clearly form a Mach cone. At higher impact speeds the fringe density was higher and the different features of the

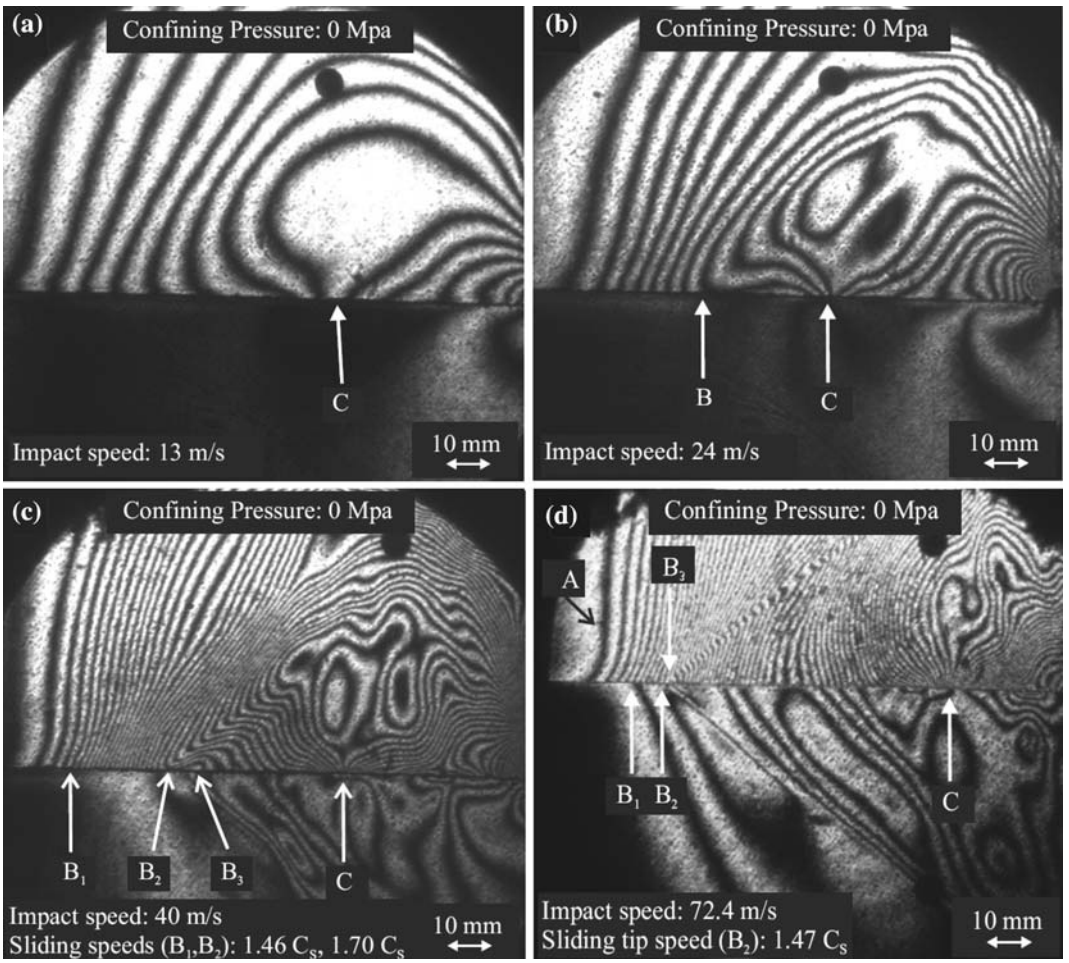

Figure 9. Representative isochromatic fringe patterns from four different experiments of sliding propagation initiated by different impact speeds. No confining stress was applied.

fringe pattern are visible. For an impact speed of 40 m/s and at 64 μs after impact the isochromatic fringes are shown in Figure 9c. The wrinkle-like structure is better defined than in the case of 24 m/s impact speed. The point C traveled along the interface at a speed of $1065\,\text{m/s} \cong 0.85\,C_S$. The fringes on the left of the wrinkle-like pulse were bent and a Mach zone was clearly emanating from the section B_2B_3. This Mach zone has an internal structure and it shows that a disturbance on the interface traveled at a supershear speed of $2118\,\text{m/s} \cong 1.7\,C_S$. Also the inclination of the fringes on the left of point B_2 is visible and a zone B_1B_2 has been formed. From the inclination angle we computed the sliding zone speed as $1830\,\text{m/s} = 1.46\,C_S$. Based on the fringe pattern we can argue that sliding started at point B_1 and the whole zone B_1B_2 propagated along the interface. We also note that the stress field in the lower plate was very low in front of the point B_2. This means that the lower plate did not interact with the upper plate and the interface did not exhibit considerable friction, which would have created, by the principle of action reaction, a significant shear stress field in the lower plate. However, it is obvious in the Figure 9c that at point B_2 the stress

field in the upper plate was disturbed and a significant stress field developed in the lower plate. It is possible to argue that the horizontal compressive stress in the upper plate increased to the right of the *p*-wave front on the side of impact. Because of the Poisson effect, this caused an increase in the vertical dynamic (inertial) compressive stress. Higher vertical compressive stress resulted in a higher friction, which created the field in the lower plate. According to the above argument, B_2B_3 was acting like a shear loading zone, which was propagated along the interface with a supershear speed. A Mach zone emerging from the area B_2B_3 is clearly visible in Figure 9c. The B_2B_3 is similar to a cohesive zone developing during shear crack propagation along glued (coherent) interfaces (Samudrala et al., 2002 a, b).

Figure 9d shows the photoelastic fringe pattern at 74 μs after impact from a projectile at a high speed of 72.4 m/s. The wave front is at A, whereas the bent fringes form a very narrow cohesive-type zone (B_2B_3). A Mach cone clearly emanates from the zone B_2B_3 at the interface and shows that a disturbance traveled along the interface with a supershear speed. The speed has been measured by means of the Mach angle and by following the positions of B_2 at different frames. The two measurements give $1943\,\text{m/s} \cong 1.55\,C_S$ and $1835\,\text{m/s} \cong 1.47\,C_S$ which are very close within a 5% experimental error. The narrow zone was detached from the wrinkle-like structure, appearing at point C of the interface (see Figure 9d). This separation verifies our conjecture that the creation of a cohesive type zone B_2B_3 is independent of the wrinkle-like pulse and it is instead related to the sliding procedure. Based again on the isochromatic fringe pattern we can argue that sliding started at point B_1.

It is clear from this investigation that the main features of the stress field (with the exception of the eye-like fringe pattern, which is associated to the loading wave) were governed by the impact speed.

6. Influence of external pressure on the sliding process

In order to investigate the influence of the external pressure on sliding, we compared three cases with very different external applied pressure and similar impact speeds in the range of 45 to 51 m/s. In Figure 10a, the initial pressure was 20 MPa and the impact speed was 45.5 m/s. We observed a complex sliding procedure (similar to the case of Figure 5, discussed extensively in Section 3). The sliding tip speed was $1859\,\text{m/s} \cong 1.49\,C_S$. A second sliding edge, which existed in the previous frames, is not shown in this picture since it already merged with the sliding edge. Comparing Figure 10a with Figure 5c, we first observe that the eye-like structure at the higher external stress had more fringes, and the compression zone AB was wider than in the case of 10 MPa confining pressure. The sliding occurred behind the sliding edge in the section BC, which was smaller than the corresponding segment BC in Figure 5c. This means that the sliding area was larger in the case of lower external pressure for the same impact speed. At 5 MPa confining external pressure (see Figure 10b), the loading structure had fewer fringes and the loading wave zone AB was decreased. The fringe structure was simpler than the fringe structure at higher confining pressures and there was not a second sliding edge. The sliding tip speed was $1.62\,C_S$.

At very low-external pressure of 1.5 MPa (Figure 10c), the eye-like fringe structure was not created. The photoelastic fringe pattern was similar to the fringe

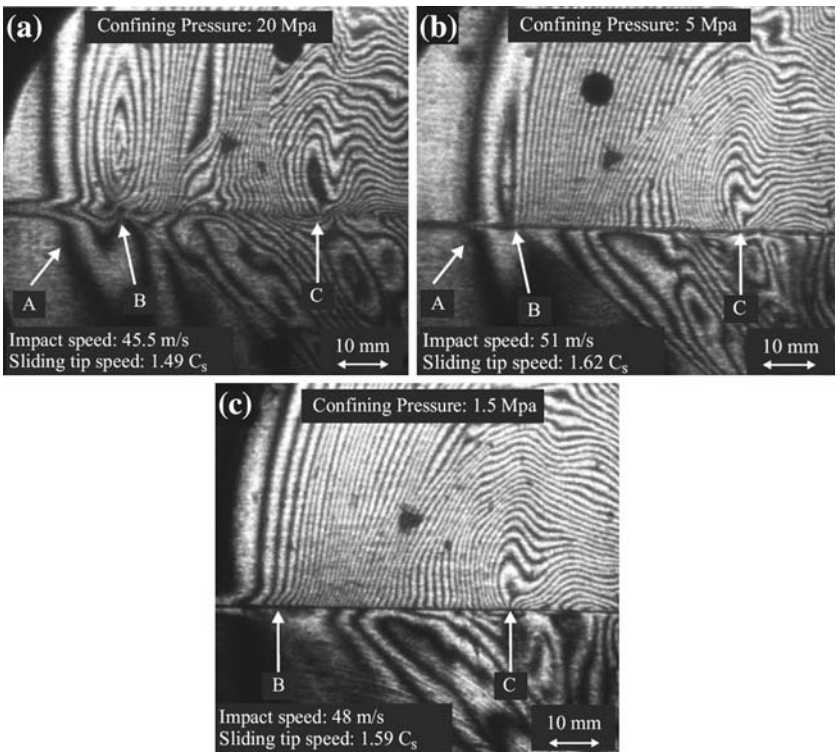

Figure 10. Representative isochromatic fringe patterns from three different experiments of sliding propagation initiated by similar high-impact speeds; the specimen was subjected to different confining stresses.

pattern developed in the case discussed extensively in Section 5, where no external pressure was applied. From the discontinuity of the fringe pattern on the interface we can conclude that at 5 and 1.5 MPa external pressure there is an extended slipping area behind the rupture point (the whole section BC is a sliding zone), which shows that the rupture mode is crack-like. These sliding zones were larger than the corresponding zones developed in the cases with higher external compressive load. We also mention that the wrinkle-like pulse was present in all cases since the impact speeds were high enough. Finally, it is noted that the sliding tip speed did not depend on the confining stress.

The results derived by an intermediate impact speed on the order of 20 m/s were similar to the results of the high-impact speeds discussed above. Because of this similarity, we will not present this case. Instead we will proceed with the case of the low-impact speed of 13 m/s (see Figure 11). In this speed range, sliding exhibits some very interesting properties.

At 10 MPa external pressure (Figure 11a), two fringe concentration points B_1 and B_2 are observed. In this case a supershear sliding pulse was generated ahead of a crack. We have presented this case in Section 4 (Figure 7b) when we investigated the influence of impact speed on sliding at constant external pressure. Another significant result is that the wrinkle-like pulse was not generated because the impact loading was too small and the detachment wave could not overcome the confining pressure. In

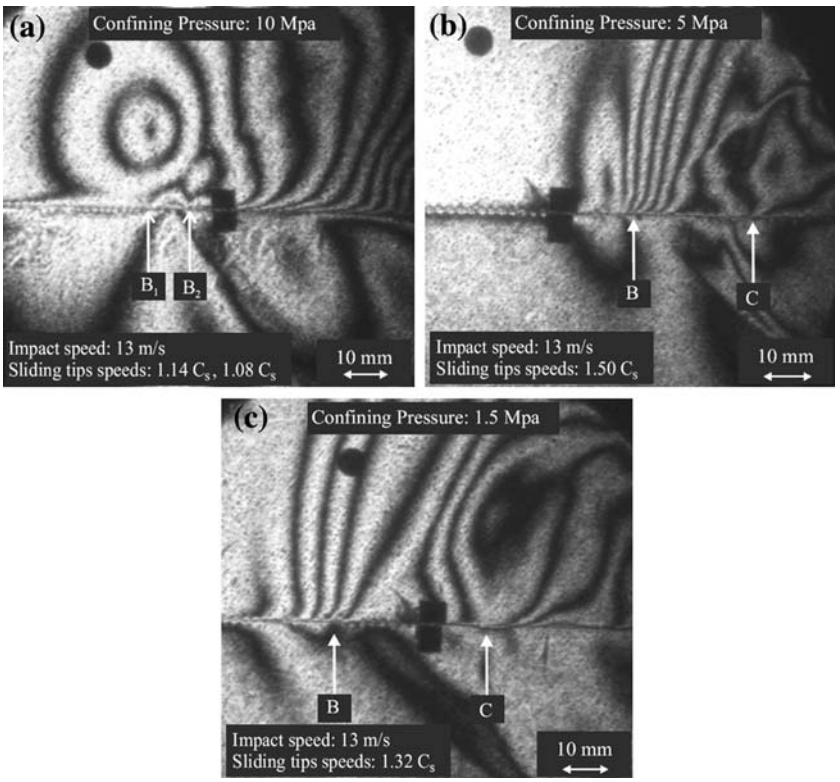

Figure 11. Representative isochromatic fringe patterns from three different experiments of sliding propagation initiated by the same low-impact speeds; the specimen was subjected to different confining stresses.

Figure 11b, the confining pressure was 5 MPa and the wrinkle-like pulse was formed; it is visible at point C. In this case the sliding tip B traveled at supershear speed of $1872\,\text{m/s} \cong 1.5\,C_S$ and the Mach cone is clearly visible. For an even smaller external pressure of 1.5 MPa, the wrinkle like interface wave was more prominent, whereas the supershear sliding tip B speed was $1655\,\text{m/s} \cong 1.32\,C_S$ (see Figure 11c).

In this section, the influence of the external confining pressure on the sliding process was discussed. Many features the stress field developed during sliding were greatly affected by the static pressure (e.g. eye-like fringe structure, length sliding section, sliding modes). We note, however, that the sliding tip speed was not dependent on the confining pressure but only on the projectile speed. Higher projectile speed resulted in higher sliding tip speed. The speed of the detachment wave was not dependent on the confining pressure nor on the projectile speed; it was always in the theoretically defined speed range (C_R, C_S).

7. Conclusions

The evolution of dynamic frictional sliding along incoherent interfaces of two identical Homalite plates, held together by compressive stress, and subjected to impact shear loading, was experimentally investigated. The case of freely standing plates

with no external pressure was also studied. The stress fields developed during the events were recorded in a microsecond time scale by high-speed photography used in conjunction with classical dynamic photoelasticity. By modifying the experimental parameters of impact speed and superimposed quasi-static pressure the following significant effects were captured:

- The interaction between the impact wave and the preexisting static stress field caused a relatively broad loading wave that emanated from the interface.
- As the projectile speed decreased under a certain value, the sliding transitioned from pure crack-like to a slip pulse followed by a crack.
- The observed propagation speeds of the sliding tips were not dependent on the confining pressure but only on the projectile speed. The speeds spanned almost the whole interval from sub-Rayleigh to nearly the p-wave speed of the material, with the exception of a forbidden gap between the Rayleigh wave speed and the shear wave speed.
- Sub-Rayleigh and intersonically propagating pulses were discovered and recorded.
- Mach lines with different inclinations emanating from the sliding zone tips were observed.
- Unlike classical shear cracks in coherent interfaces of finite strength, sliding areas in frictional interfaces seem to grow without noticeable acceleration phases and at various discrete speeds.
- Behind the sliding tip, wrinkle-like pulses were identified that traveled always (independently of the impact speed or the confining stress) at speeds between the Rayleigh wave speed and the shear wave speed of the material, were identified.
- There was a cusp in the stress contours at the interface, indicating that the propagation speed was slightly faster along the interface than in the bulk.

Acknowledgments

The authors gratefully acknowledge the support of the Office of Naval Research through grant N00014-03-1-0435 (Dr. Y.D.S. Rajapakse, project monitor).

References

Abraham, F.F. and Gao, H.J. (2000). How fast can cracks propagate? *Physical Review Letters* **84**, 3113–3116.

Abraham, F.F. (2001). The atomic dynamics of fracture. *Journal of the Mechanics and Physics of Solids* **49**, 2095–2111.

Achenbach, J.D. and Epstein, H.I. (1967). Dynamic interaction of a layer and a half-space. *Journal of Engineering Mechanics* **5**, 27–42.

Adams, G. (1998). Steady sliding of two elastic half-spaces with friction reduction due to interface stick-sip. *Journal of Applied Mechanics* **65**, 470–475.

Andrews, D.J. and Ben-Zion, Y. (1997). Wrinkle-like slip pulse on a fault between different materials. *Journal of Geophysical Research* **102**, 553–571.

Anooshehpoor, A. and Brune, J.N. (1999). Wrinkle-like Weertman pulse at the interface between two blocks of foam rubber with different velocities. *Geophysical Research Letters* **23**, 2025–2028.

Archuleta, R.J. (1984). A faulting model for the 1979 Imperial Valley earthquake. *Journal of Geophysical Research* **89**, 4559–4585.

Ben-Zion, Y. (2001). Dynamic ruptures in recent models of earthquake faults. *Journal of the Mechanics and Physics of Solids* **49**, 2209–2244.

Ben-Zion, Y. and Huang, Y. (2002). Dynamic rupture on an interface between a compliant fault zone layer and a stiffer surrounding solid. *Journal of Geophysical Research* **107**, No B2, 10.1029/2001JB000254.

Bouchon, M., Bouin, M.P., Karabulut, H., Toksoez, M.N., Dietrich, M. and Rosakis, A.J. (2001). How fast is rupture during an earthquake? New sights from the 1999 Turkey earthquakes. *Geophysical Research Letters* **28**, 2723–2726.

Bouchon, M. and Vallee, M. (2003). Observation of long supershear rupture during the magnitude 8.1 Kunlunshan earthquake. *Science* **301**, 824–826.

Broberg, K.B. (1999). *Cracks and fracture*. Academic Press, London.

Burridge, R., Conn, G. and Freund, L.B. (1979). The stability of rapid mode II shear crack with finite cohesive traction. *Journal of Geophysical Research* **84**, 2210–2222.

Cochard, A. and Rice, J.R. (2000). Fault rupture between dissimilar materials: Ill-posedeness, regularization, and slip-pulse response. *Journal of Geophysical Research* **105**, 25891–25897.

Coker, D. and Rosakis, A.J. (2001). Experimental observations of intersonic crack growth in asymmetrically loaded unidirectional composite plates. *Philosophical Magazine A* **81**, 571–595.

Coker, D., Lykotrafitis, G., Needleman, A. and Rosakis, A.J. (2005). Frictional sliding modes along an interface between identical elastic plates subject to shear impact loading. *Journal of the Mechanics and Physics of Solids* **53**(4), 884–922.

Comninou, M. and Dundurs, J. (1977). Elastic interface waves involving separation. *Journal of Applied Mechanics, ASME* **44**, 222–226.

Das, S. (1985). Application of dynamic shear crack models to the study of the earthquake faulting process. *International Journal of Fracture* **27**, 263–276.

Dieterich, J.H. (1979). Modeling of rock friction 1. Experimental results and constitutive equations. *Journal of Geophysical Research* **84**, 2161–2168.

Ellsworth, W.L., Celebi, M., Evans, J.R., Jensen, E.G., Kayen, R., Metz, M.C., Nyman, D.J., Roddick, J.W., Spudich, P. and Stephens, C.D. (2004). Near-field ground motion of the 2002 Denali Fault, Alaska, earthquake recorded at pump station 10. *Earthquake Spectra* **20**, 597–615.

Freund, L.B. (1979). The mechanics of dynamic shear crack propagation. *Journal of Geophysical Research* **84**, 2199–2209.

Freund, L.B. (1990). *Dynamic Fracture Mechanics*. Cambridge, UK.

Gao, H.J., Huang, Y. and Abraham, F.F. (2001). Continuum and atomistic studies of intersonic crack propagation. *Journal of the Mechanics and Physics of Solids* **49**, 2113–2132.

Hao, S., Wing, K.L., Klein, P.A. and Rosakis, A.J. (2004). Modeling and simulation of intersonic crack growth. *International Journal of Solids and Structures* **41**, 1773–1799.

Heaton, T.H. (1990). Evidence for and implications of self-healing pulses of slip in earthquake rupture. *Physics of The Earth and Planetary Interiors* **64**, 1–20.

Hernandez, B., Cotton, F. and Campillo, M. (1999). Contribution of Radar interferometry to a two-step inversion of the kinematic process of the 1992 Landers earthquake. *Journal of Geophysical Research* **104**, 13083–13099.

Ibrahim, R.A. (1994). Friction-induced vibration, chatter, squeal, and chaos, Part I: Mechanics of contact and friction. *Applied Mechanics Reviews ASME* **47**, 209–226.

Lin, A., Guo, J., Zeng, Q., Dang, G., He, W. and Zhao, Y. (2002). Co-Seismic strike-slip and rupture length produced by the 2001 M_S 8.1 central Kunlun earthquake. *Science* **296**, 2015–2017.

Linker, M.F. and Dieterich, J.H. (1992). Effects of variable normal stress on rock friction: observations and constitutive equations. *Journal of Geophysical Research* **97**, 4923–4940.

Needleman, A. (1999). An analysis of intersonic crack growth under shear loading. *Journal of Applied Mechanics ASME* **66**, 847–857.

Nielsen, S. and Madariaga, R. (2003). On the self-healing fracture mode. *Bulletin of The Seismological Society of America* **93**, 2375–2388.

Olsen, K.B., Madariaga, R. and Archuleta, R.J. (1997). Three-dimensional dynamic simulation of the 1992 Landers earthquake. *Science* **278**, 834–838.

Prakash, V. and Clifton, R.J. (1993). Pressure-shear plate impact measurement of dynamic friction for high speed machining applications. *Proc. 7th International Congress on Experimental Mechanics*. Society of Experimental Mechanics, Bechtel, CT, pp. 556–564.

Prakash, V. (1998). Frictional response of sliding interfaces subjected to time varying normal pressures. *Journal of Tribology ASME* **120**, 97–102.

Ranjith, K. and Rice, J.R. (2001). Slip dynamics at an interface between dissimilar materials. *Journal of the Mechanics and Physics of Solids* **49**, 341–361.

Rice, J.R. and Ruina, A.L. (1983). Stability of frictional sliding. *Journal of Applied Mechanics* **50**, 343–349.

Rice, J.R. (2001). New perspectives on crack and fault dynamics. In *Mechanics for a New Millennium*, (edited by Aref, H. and Philips, J. W.,) Kluwer Academic Publishers, Dordrecht, pp. 1–23.

Rice, J.R., Lapusta, N. and Ranjith, K. (2001). Rate and state dependent friction and the stability of sliding between elastically deformable solids. *Journal of the Mechanics and Physics of Solids* **49**, 1865–1898.

Rosakis, A.J., Samudrala, O. and Coker, D. (1999). Cracks faster than the shear wave speed. *Science* **284**, 1337–1340.

Rosakis, A. J. (2002). Intersonic shear cracks and fault ruptures. *Advances in Physics* **51**(4), 1189–1257.

Rubinstein, S., Cohen, G. and Fineberg, J. (2004). Detachment fronts and the onset of dynamic friction. *Nature* **430**, 1005–1009.

Ruina, A.L. (1983). Slip instability and state variable friction laws. *Journal of Geophysical Research* **88**, 10359–10370.

Samudrala, O., Huang, Y. and Rosakis, J.R. (2002a). Subsonic and intersonic mode II crack propagation with a rate-dependent cohesive zone. *Journal of the Mechanics and Physics of Solids* **50**, 1231–1268.

Samudrala, O., Huang, Y. and Rosakis, A.J. (2002b). Subsonic and intersonic shear rupture of weak planes with a velocity weakening cohesive zone. *Journal of Geophysical Research* **107**, No B8, 10129/2001JB000460.

Samudrala, O. and Rosakis, A.J. (2003). Effect of loading and geometry on the subsonic/intersonic transition of a bimaterial interface crack. *Engineering Fracture Mechanics* **70**, 309–337.

Schallamach, A. (1971). How does rubber slide? *Wear* **17**, 301–312.

Weertman, J. (1980). Unstable slippage across a fault that separates elastic media of different elastic constants. *Journal of Geophysical Research* **85**, 1455–1461.

Xia, K., Rosakis, A. J. and Kanamori, H. (2004). Laboratory earthquakes: the sub-Rayleigh-to-supershear rupture transition. *Science* **303**, 1859–1861.

Xia, K.W., Rosakis A.J., Kanamori H. and Rice J.R. (2005). In homogeneous faults hosting earthquakes in the laboratory: directionality and supershear. *Science* **308**, 681–684.

Zheng, G. and Rice, J.R. (1998). Conditions under which velocity-weakening friction allows a self-healing versus a crack-like mode of rupture. *Bulletin of the Seismological Society of America* **88**, 1466–1483.